Atmospheric Research 226 (2019) 1–16

Contents lists available at ScienceDirect

Atmospheric Research

journal homepage: www.elsevier.com/locate/atmosres

Improving WRF model turbine-height wind-speed forecasting using a surrogate- based automatic optimization method

Zhenhua Di[a], Juan Ao[b], Qingyun Duan[a,*], Jin Wang[b], Wei Gong[a], Chenwei Shen[a], Yanjun Gan[c], Zhao Liu[b]

[a] State Key Laboratory of Earth Surface Processes and Resource Ecology, Faculty of Geographical Science, Beijing Normal University, Beijing 100875, China
[b] Beijing Goldwind Science & Creation Windpower Equipment Co., Ltd., Beijing 100176, China
[c] State Key Laboratory of Severe Weather, Chinese Academy of Meteorological Sciences, Beijing 100081, China

ARTICLE INFO

Keywords:
WRF
Parameter optimization
Surrogate modeling-based optimization
Turbine-height wind-speed forecasting

ABSTRACT

Improving turbine-height wind-speed forecasting using a mesoscale numerical weather prediction (NWP) model is important for wind-power prediction because of the cubic correlation between wind power and wind speed. This study investigates how a surrogate-based automatic optimization method can be used to improve wind-speed forecasting by an NWP model by optimizing its parameters. A key challenge in optimizing NWP model parameters is the tremendous computational requirements of such an exercise. A global sensitivity method known as the Multivariate Adaptive Regression Spline (MARS) method was first used to identify the most sensitive parameters among all tunable parameters chosen from seven physical parameterization schemes of the Weather Research and Forecast (WRF) model. Then, a highly effective and efficient optimization method known as adaptive surrogate modeling-based optimization (ASMO) was used to tune the sensitive parameters. In a case study carried out over Eastern China, the seven parameters that were most sensitive to wind-speed simulation were identified from among 27 tunable parameters. Those seven parameters were optimized using the ASMO method. The present study indicates that the hourly wind-speed simulation accuracy was improved by 8.7% during the calibration phase and by 7.58% during the validation phase. In addition, clear physical interpretations were provided to explain why the optimal parameters lead to improved wind speed forecasts. Overall, this study has demonstrated that automatic optimization method is a highly effective and efficient way to improve wind-speed forecasting by an NWP model.

1. Introduction

With the rapid growth of the global economy, consumption of traditional fossil fuels such as coal and oil has soared, leading to an energy source depletion crisis. The resulting environmental problems such as air and water pollution are becoming critical (Boffey, 1970). Development of renewable energy resources is thought to be the most promising response because these resources are basically inexhaustible, offer huge capacity, and are clean, with very little pollution. Due to its wide distribution, wind energy, as the major renewable energy resource available, has been widely used to generate electricity around the world (Grubb and Meyer, 1993; National Renewable Energy Laboratory, 2008; Lu et al., 2009; Moemken et al., 2018).

Wind turbines have usually been built on mountain tops or in coastal areas with strong wind. The turbine rotor is installed at a height above the tower bottom (usually the ground surface) ranging from 70 to 110 m, which is called the turbine height in this study. The turbine-height wind speed is a critical variable affecting the amount of wind-generated electricity that can be produced. When the turbine-height wind speed is between 3 and 15 m s^{-1}, wind electricity generation starts, and the corresponding electric power production is approximately a cubic function of wind speed (Jaramillo and Borja, 2004; Yang et al., 2017). This implies that wind-power (i.e., wind-generated electric power) estimation accuracy relies mainly on the accuracy of turbine-height wind-speed forecasting. Additionally, when the wind speed is > 15 m s^{-1}, and especially higher than 20–25 m s^{-1}, the turbine components will be damaged due to excessive power inputs, which disturb the stable operation of the wind-powered electrical generation system and cause huge economic losses. The best solution is to shut down the turbines before strong winds arrive. Therefore, the forecasting accuracy of turbine-height wind speed is becoming very important for the accurate evaluation of wind power and the safe operation of wind-

* Corresponding author at: Beijing Normal University, NO.19, Xinjiekouwai Street, Haidian District, Beijing, China.
E-mail address: qyduan@bnu.edu.cn (Q. Duan).

https://doi.org/10.1016/j.atmosres.2019.04.011
Received 10 December 2018; Received in revised form 8 April 2019; Accepted 9 April 2019
Available online 11 April 2019
0169-8095/

powered electrical generation systems in wind farms.

Wind-speed forecasting methods include statistical estimation methods and physical model-based simulation methods. Common statistical estimation methods include predictive time-series models built using Kalman filters (Bossanyi, 1985) or autoregressive moving average functions (Sfetsos, 2002) and correlation models built using artificial neural networks (Mohandes et al., 1998) or fuzzy logic (Pinson et al., 2003). The predictive accuracy of these statistical models depends strongly on the reliability of past data observations and the number of observed data points. In addition, statistical models tend to have a short prediction lead time, usually six to eight hours. Unlike statistical models, physical model-based mesoscale numerical weather prediction (NWP) models have significant advantages for operational forecasting of turbine-height wind speed. An NWP model not only is less dependent on observed data and therefore can compensate for data deficiencies, especially in complex terrain, but also has a longer forecast period, with 72-h prediction accuracy > 80%. In recent decades, mesoscale NWP models have been widely used to provide high-resolution wind-speed forecasts. For instance, Lazić et al. (2010) assessed the performance of the Eta model on the wind forecasts for the Nasudden power plants at Gotland Island, Sweden. Dvorak et al. (2010) used the National Center for Atmospheric Research Mesoscale Model version 5 (MM5) model to simulate multi-year high-resolution wind speed at 80 m to assess the wind energy resource in offshore California.

The Weather Research and Forecasting (WRF) model (Skamarock et al., 2008) is a new- generation mesoscale NWP model developed on the basis of the MM5 model. It has a modular structure that facilitates integration of various physical process modules, and each physical module has been developed by a different group (Dudhia, 2014). Recently, more and more studies have evaluated turbine-height wind speed using the WRF model. Deppe et al. (2013) evaluated the simulation ability of the WRF model on 80 m turbine-height wind speed at the Pomeroy, Iowa wind farm site in United States. Hahmann et al. (2015) found that the biases in mean annual wind speed between WRF simulations and observations at heights around 100 m were far smaller than those obtained by using winds directly from the reanalysis at offshore sites over the North and Baltic Seas. However, small biases in simulated wind speed have a significant effect on wind-power prediction accuracy because of the cubic relationship between wind power and turbine-height wind speed. Moreover, the WRF simulation has significant errors of its own due to its imperfect descriptions of sub-grid physical processes and topography. Improving the simulation accuracy of turbine-height wind speed in the WRF model is therefore of critical importance.

As in other numerical models, there are three main sources of uncertainty in the WRF model: the specification of initial and boundary fields, the realism of the model physics representation, and the specification of model parameters (Di et al., 2015). To reduce initial and boundary errors, three- and four-dimensional variation data assimilation (3DVAR/4DVAR) methods are used to improve the specification of initial and boundary fields for the WRF model by ingesting discrete observational data from diverse sources. Wang et al. (2013) improved the surface-layer wind forecasting accuracy of the WRF model in a wind-power farm using the 3DVAR method. Fan et al. (2013) assimilated quick scatterometer ocean-surface wind data into a WRF model using the 3DVAR method to obtain a high-quality simulation of the surface wind field in the Chukchi/Beaufort Sea region.

To reduce errors in WRF physical representations, many studies have analyzed the representativeness of various physical parameterization schemes for the simulation of the physical processes related to wind. Fernández-González et al. (2019) analyzed the WRF uncertainty associated with the multiphysics and the multiple initial and boundary condition for the short-term wind speed prediction, and found that the physical parameterization uncertainty was greater for short-term wind forecasts. Some studies built WRF ensemble forecasting systems to improve the wind speed and direction forecasts using several sets of parameterization scheme combinations (Traiteur et al., 2012; Fernández-González et al., 2018; Pan et al., 2018). Noted that the ensemble forecasting accuracy would be further improved using a more advanced post-processing technique (Holman et al., 2018); some other studies focused on the sensitivity of the different boundary layer schemes to wind forecasts to quantify their suitable boundary layer schemes (Hariprasad et al., 2014; Avolio et al., 2017; Tymvios et al., 2018; Xiang et al., 2019).

However, very little research has been done on parameter optimization to improve turbine-height wind-speed forecasting in the WRF model. The key challenge includes two aspects: (1) the WRF model has many tunable parameters, which makes parameter optimization difficult if all parameters are adjusted; and (2) a WRF run is very expensive, which makes it difficult to find the optimal parameter values for traditional optimization methods because of relatively low search efficiency. Therefore, a highly efficient optimization method should be used to conduct parameter optimization of a complex WRF model. To perform parameter optimization for the complex dynamic models such as WRF, two steps are recommended (Di et al., 2015). The first is to conduct parameter screening using a sensitivity analysis (SA) method to choose the sensitive parameters to be optimized. Not all parameters are sensitive to the WRF outputs (e.g., the turbine-height wind speed), and if the insensitive parameters are calibrated, not only is the WRF simulation accuracy not significantly improved, but also the huge computation resources are wasted. Many studies have evaluated parameter sensitivity for complex weather and climate models using qualitative and quantitative SA methods (Qian et al., 2015; Di et al., 2017). These results have demonstrated that the Multivariate Adaptive Regression Spline (MARS) method is a very effective and efficient qualitative SA method to identify the sensitive parameters.

Once the sensitive parameters have been determined, the next step involves conducting an optimization of these parameters. However, the efficiency of traditional optimization methods is still low even for optimizing the sensitive parameters as a small proportion of all tunable parameters. Therefore, a more highly effective and efficient optimization method should be used. Wang et al. (2014) proposed an adaptive surrogate modeling-based optimization (ASMO) method by combining the more suitable Gaussian Processes regression method and the shuffled complex evolution (SCE-UA) global optimization algorithm. Duan et al. (2017) first conducted highly efficient parameter optimization for the WRF model to improve the accuracy of summer precipitation simulation in the Greater Beijing area using the ASMO method developed by Wang et al. (2014). Finally, the accuracy of precipitation simulation was improved by approximately 18% using only 127 model runs. More recently, the ASMO method has been applied to parameter optimization of complex land and weather models (Gong et al., 2015; Di et al., 2018). However, the ASMO method has not yet been applied to parameter optimization for the WRF model to improve the simulation accuracy of turbine-height wind speed.

The present work intends to implement a highly effective and efficient parameter optimization strategy including MARS-based parameter SA and ASMO-based sensitivity parameter optimization for the WRF model to improve turbine-height wind-speed simulation. The reasonableness and applicability of the optimal parameters obtained by the ASMO method will then be assessed.

This paper is organized as follows. Section 2 presents the methodology, including the MARS SA method and the ASMO optimization procedure. Section 3 describes the experiment design, including the simulation design, the tunable parameters, and the statistical metrics. Section 4 first presents the results of the sensitive parameters in brief and then presents analyses of the optimization results, including the optimization efficiency and accuracy improvement for wind-speed and wind-power simulations. Comparisons of validation event simulations and physical interpretations of why the optimal parameters lead to improved wind-speed forecasts are also described in this section to provide further proof of the reasonableness and applicability of the

optimal parameters obtained. Conclusions are presented in the last section.

2. Materials and methods

An integrated parameter optimization procedure for complex dynamic models such as WRF should consist of two steps. First, parameter SA should be conducted for all tunable parameters using an SA method to screen a small number of sensitive parameters. Second, the screened sensitive parameters should be optimized using a highly effective and efficient parameter optimization method instead of more traditional optimization methods.

2.1. Good lattice point (GLP) sampling method

Uniformity is one of the important indices for sampling methods because uniform samples help to obtain more accurate parametric SA and optimization results. The uniformities of three categories of quasi-Monte-Carlo methods, including the GLP method, the Halton sequence, and the Sobol' sequence, have been compared by Gong et al. (2016), who demonstrated that the GLP method has higher uniformity than the other two methods with the same sample size. Therefore, GLP sampling methods are recommended to generate uniform samples for further SA and ASMO methods.

The GLP method was first proposed by Korobov (1959a), and its design can be briefly described as follows. Let $(n; h_1, \ldots, h_s)$ be a vector of integers satisfying $1 \le h_i < n$, $h_i \ne h_j$ for $i \ne j$, $s < n$, such that the greatest common divisor of h_i and n is 1. The components of the sample are constructed according to Eq. (1):

$$x_{ki} = \frac{2kh_i(\mathrm{mod}\, n) - 1}{2n}, \quad i = 1, \cdots, s, \quad k = 1, \cdots, n \tag{1}$$

The point set $P_n = \{X_k = (x_{k1}, \ldots, x_{ks}), k = 1, \ldots, n\}$ is called the lattice point set of the generating vector $(n; h_1, \ldots, h_s)$. If the sequence P_n has the lowest discrepancy, the set P_n is called a GLP set. Obviously, finding the best integer vector $(n; h_1, \ldots, h_s)$ to ensure that the associated set P_n has the lowest discrepancy requires a large amount of computation. To solve this problem, Korobov (1959b) proposed a power vector instead of an integer vector to easily obtain the GLP set P_n.

2.2. MARS SA method

The MARS method (Friedman, 1991) has been widely used to construct the statistical regression model between perturbed parameter inputs and the corresponding simulated outputs. The process includes two phases: the forward and the backward pass. The forward pass usually involves building an overfitted model by repeatedly adding the basis functions in pairs. The basis function contains three types of expression: a constant, a hinge function, and the product of several hinge functions. Then, the backward pass prunes the overfitted model to the best model by repeatedly deleting the least effective term. The backward pass uses generalized cross validation (GCV) to measure the performance of model subsets for obtaining the best model. The GCV formula can be expressed as follows:

$$GCV(M) = \frac{\frac{1}{N}\sum_{i=1}^{N}\left(Y_i - \hat{Y_i}\right)^2}{\left[1 - \frac{1 + c(M)d}{N}\right]^2} \tag{2}$$

where N is the number of samples, Y_i is the data point i, $\hat{Y_i}$ is the estimated value of Y_i based on the MARS regression model M, d is the effective degrees of freedom, and $c(M)$ is a penalty factor when adding a basis function. A lower GCV value represents a better-fitted model.

Once the MARS regression model has been built, GCV can be used as an SA index to evaluate parameter sensitivity. Each parameter is deleted once, one at a time, from the model. When a certain parameter is deleted from the best MARS regression model, the absolute increment of GCV is the largest, which indicates that the removed parameter is the most sensitive. Specifically, the parametric sensitivity scores are obtained as follows. First, the tunable parameter space is sampled using a sampling method to obtain perturbed parameter values, and the corresponding simulation errors are evaluated by substituting the perturbed values into the model. Then, the suitable MARS regression model is built using the perturbed parameter values and their simulation errors, and its GCV value is evaluated using Eq. (2). Finally, compared with the GCV of the MARS model, the absolute increment of GCV for each parameter is evaluated when the parameter is removed from the MARS expression. All parameter GCV increments are normalized by dividing them by the sum of all GCV increments. The normalized GCV increment of the parameter represents its sensitivity score. The higher the score, the greater is the sensitivity.

2.3. ASMO parameter optimization method

Compared to the traditional parameter optimization method, the ASMO method (Wang et al., 2014) has higher search efficiency for finding the optimal parameters. This is because the ASMO method uses the shape information of the statistical response surface (also called the statistical regression surface) to help find the optimization area of the model response quickly. Moreover, searches mainly occur in the statistical response surface model, reducing the number of physical model runs. The specific ASMO procedure for WRF parameter estimation can be summarized as follows:

i. Sample the tunable parameter space to generate representative parameter sets using suitable sampling methods. Then substitute these representative parameter sets into the WRF model to run the model to obtain the corresponding simulation errors of the variable (e.g., wind speed). Combine the input perturbed parameter sets and the corresponding output errors to constitute the set of initial sample points.
ii. Build a statistical surrogate model based on the initial sample points using a suitable Gaussian Processes regression method. Note that the curve surface of the statistical surrogate model should pass through all the initial sample points, ensuring that the statistical model provides a close approximation to the real WRF response surface model.
iii. Search for the optimal parameters on the surrogate model using the global rapid SCE-UA optimization method (Duan et al., 1994). Then the new parameter set (i.e., the optimal parameters of the surrogate model) is substituted into the WRF physical model to evaluate the corresponding output error. Generate a new sample point consisting of the new parameter set and its WRF output error. Next, update the initial sample points by adding the newly generated sample point.
iv. Repeat steps ii and iii until the optimization convergence criteria are met, at which point the globally optimal parameter values of the real WRF physical model have finally been found. The optimization convergence criteria is usually defined as the local optimal value remaining unchanged after a series of searches equal to five to ten times the parameter dimensionality, or the number of searches reaching the prescribed maximum number of samples.

3. Experimental design

3.1. Model and simulation design

To obtain high spatiotemporal resolution wind-speed forecasts, a mesoscale NWP model must be used. This study uses the Advanced Research Weather Research and Forecasting model Version 3.7.1 (WRF-ARW Version 3.7.1, http://www2.mmm.ucar.edu/wrf/users).

The study area is located at the junction of five provinces (Henan, Hubei, Hunan, Anhui, and Jiangxi) within 28.83°–33.80°N and

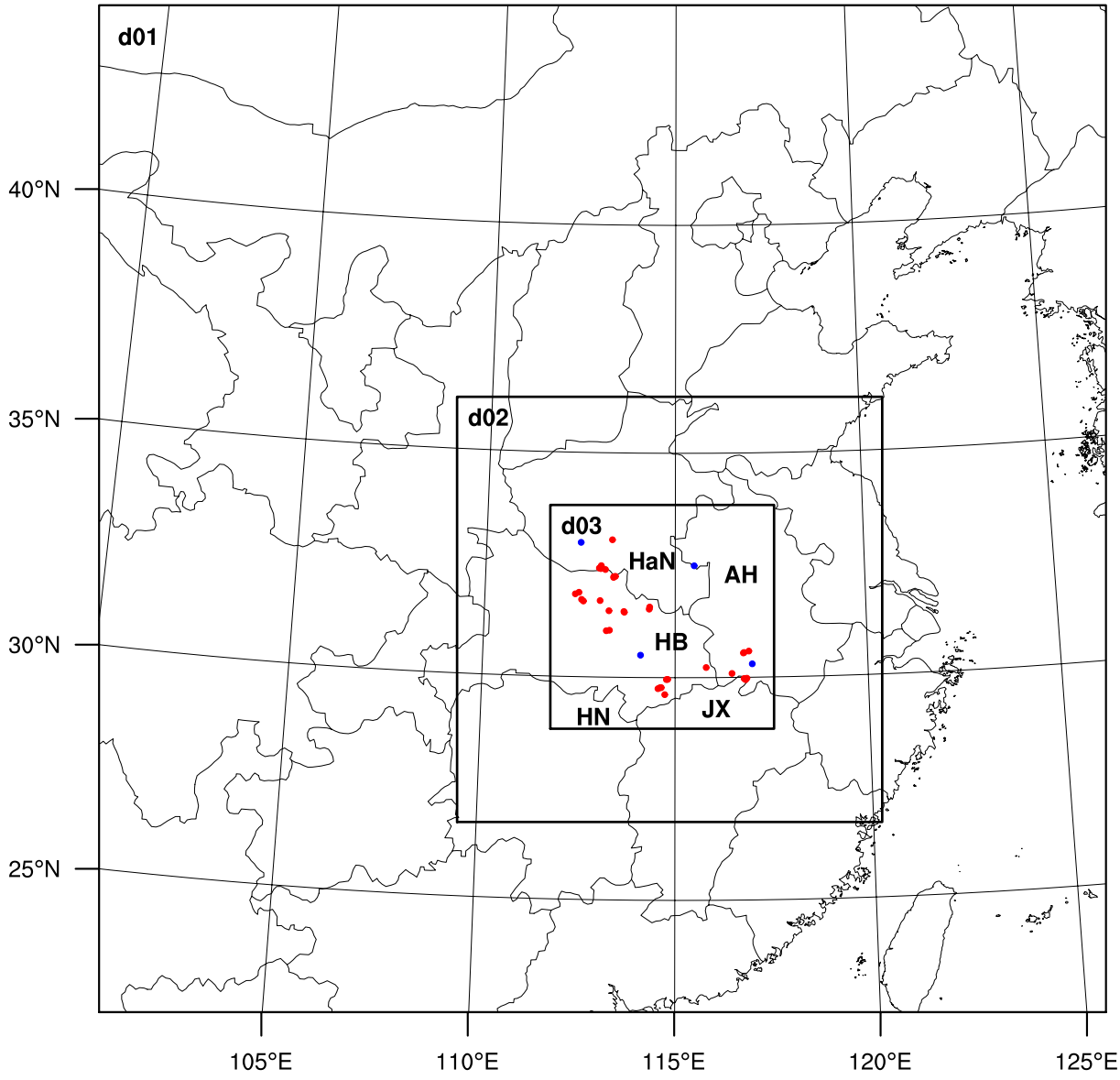

Fig. 1. The three-grid horizontally nested domain, with *d01* containing the outer grids, *d02* containing the intermediate grids cell, and *d03* containing the inner girds cells encompassing the junction of the five provinces of Henan (HaN), Anhui (AH), Hubei (HB), Hunan (HN), and Jiangxi (JX) in Eastern China. Red dots represent the observation stations for turbine-height wind speed, and blue dots represent the sounding stations. (For interpretation of the references to colour in this figure legend, the reader is referred to the web version of this article.)

111.82°–117.52°E over Eastern China (the d03 area in Fig. 1), where wind energy resources are abundant, and therefore many wind-measurement stations have been built in regions with many wind farms (usually on mountain tops). To obtain more accurate turbine-height wind-speed simulations for the study area, a three-grid, horizontally nested simulation area has been designed (see Fig. 1). The outer, intermediate, and inner layers (i.e., the *d01*, *d02*, and *d03* domains in Fig. 1) have horizontal resolutions of 27, 9, and 3 km, with the numbers of grid cells being 90 × 90, 114 × 114, and 180 × 180 respectively. The function of the *d01* and *d02* simulation domains is to provide more accurate initial and lateral boundary forcing data for simulation of the *d03* domain. Initial and lateral boundary data for the outer layer (i.e., the *d01* domain) are obtained from the National Center for Environmental Prediction (NCEP). Reanalysis data have 1° × 1° horizontal resolution and a 6-hourly interval. The vertical domain is divided into 38 sigma layers from the ground surface up to 50 hPa for the three nested domains. The uniform time step is 180 s.

Thirty-one wind-site stations marked with red dots measuring turbine-height wind speeds and four sounding stations marked with blue dots measuring wind and temperature profiles are used to provide observed data to evaluate the corresponding WRF simulation results (Fig. 1). In this study, wind data at the turbine heights of 70 or 80 m from the ground surface are used.

The simulation period for turbine-height wind speed using the WRF model spans eight individual weather processes arranged into four seasons (spring, summer, fall, and winter) in one year from June 2014 to May 2015. Fig. 2 shows the eight selected wind processes (Fig. 2a–h). Each season includes two processes (i.e., Fig. 2a and b in summer, Fig. 2c and d in fall, Fig. 2e and f in winter, and Fig. 2g and h in spring). For each process, the wind speed experiences a small–big–small variation, and the wind direction experiences an approximately south–-north–south variation. To obtain better WRF simulation results, each weather process lasting 6 days is divided into two 3-day events to be simulated separately. For example, for weather process in Fig. 2a experienced from 18 to 24 June 2014, two 3-day simulation events are defined, one extending from 18 to 21 June and the other from 21 to 24

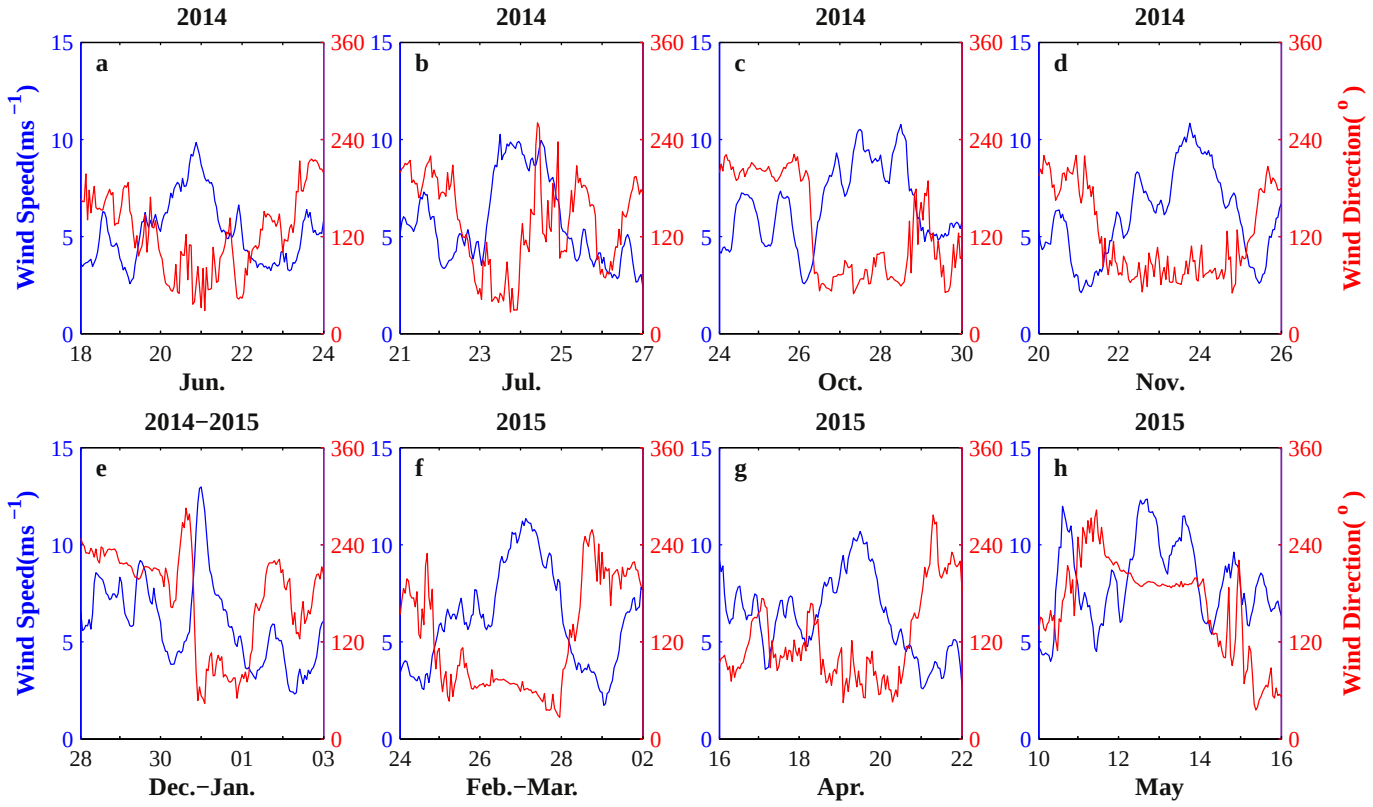

Fig. 2. The eight wind processes, including variations in wind speed and direction.

June. To reduce the effect of initial errors, the simulation of each 3-day event lasts up to 84 h, including a preceding 12-h initialization period. Overall, 16 events are simulated, and each event lastes 3 days. According to the sequential order of the eight processes as shown in Fig. 2, the corresponding 16 events marked as (1)–(16) are determined and simulated to demonstrate the WRF model parameter optimization results.

3.2. Tunable parameters from seven physical parameterization schemes

The description of the physical framework of the WRF model includes seven main physical processes: near-surface physics, cumulus convection, microphysics, long-wave and short-wave processes, land-surface physics, and planetary boundary layer physics. Each physical process can be represented by several parameterization schemes. In this study, a suite of fixed parameterization schemes is chosen to comply with the operational forecasting choice of the China Meteorological Administration for turbine-height wind-speed simulation. The specific WRF parameterization schemes are the Monin-Obukhow surface-layer scheme (Dudhia et al., 1999), the Kain-Fritsch (new Eta) cumulus scheme (Kain, 2004), the Goddard microphysics scheme (Tao and Simpson, 1993), the rapid radiative-transfer model for the GCM long-wave/shortwave scheme (Iacono et al., 2008), the Yonsei University planetary boundary layer scheme (Hong et al., 2006), and the Noah land-surface scheme (Chen and Dudhia, 2001).Twenty-seven tunable parameters are selected from the seven fixed parameterization schemes and are listed in Table A.1 of Appendix A. Note that many parameters were named according to their parameterization schemes, such as *convection_1*, *microphys_2*, and *radiation_3*. This has been done because these parameters are presented in the schemes in the form of added scale factors or specific values, not to be named by model developers.

The tunable parameters are determined based on a review of the literature and a careful examination of related program codes. After this, the parameter ranges are specified as follows. If no guidance is available, the parameter ranges are determined by multiplying their default values by factors of 0.5 and 1.5. This method has been used for specifying parameter ranges in some papers in the literature (e.g., Zhang and Anthes, 1982; Yang et al., 2017). Table A.1 shows that most of the parameters have their ranges determined according to the factors 0.5 and 1.5.

If the parameter ranges could be found in the literature or in related scheme codes, they are used in this study. For example, the parameter ranges for the cumulus scheme are obtained based on Yang et al. (2012), in which the physical interpretations of the parameter ranges are also given; *surface_1* represents the scaling factor of surface roughness, and its range is set to 1–2 following Mass and Ovens (2010), who found that WRF generally has a substantial overestimation bias at low or moderate wind-speed resolution, which could be corrected by increasing the surface roughness (or *surface_1*). Here, karman (i.e, the von Kármán constant) is viewed as a universal constant that applies to both the surface-layer and planetary-boundary layer schemes, although it is listed in the parameter set of the surface-layer scheme in Table A.1. Therefore, the range of karman is set to 0.35–0.4 as suggested by Stull (1988). The radiation_2 parameter represents the scaling factor related to cloud single-scattering albedo. If the parameter value is too large, there will be a high probability that the cloud albedo is > 1, which leads to a parameter value with no physical significance. Therefore, the range of radiation_2 is set to 0.5–1.0. The *radiation_3* parameter is a scaling factor related to the diffusivity angle of cloud optical depth, and its range is set to 0.9–1.08 based on the limits on the range of diffusivity angle in the program code. The parameter ranges are determined based on a comprehensive analysis of parameter perturbations and are therefore thought to be suitable for performing SA under all wind conditions. Moreover, the sixteen calibration events are selected from four seasons of one year, which also demonstrates that the parameter ranges are suitable to different seasons.

3.3. Statistical metrics

The statistical metrics used to evaluate wind-speed simulations are the root mean square error (*RMSE*), the correlation coefficient (*R*), and the Weibull probability density function. Another statistical metric used to evaluate average wind power is wind power density (WPD).

RMSE can be expressed as follows:

$$RMSE = \sqrt{\frac{\sum_{t=1}^{T}\sum_{i=1}^{M}(sim_i^t - obs_i^t)^2}{MT}} \tag{3}$$

where sim_i^t and obs_i^t represent the simulated and observed turbine-height wind speed at the *i*th observation station at time *t*, and *M* and *T* are the total numbers of observation stations and time steps.

To provide a better optimization result for multi-event cases, the normalized *RMSE* (*NRMSE*) is usually used as the cost function; its formula can be expressed as follows:

$$NRMSE_i = \frac{1}{N}\sum_{i=1}^{N}\frac{RMSE_p^i}{RMSE_{def}^i} \tag{4}$$

where $RMSE_p^i$ represents the *RMSE* value of the simulation with the perturbed parameter value for the *i*th event and $RMSE_{def}^i$ represents the *RMSE* value of the simulation with the default parameter value for *i*th event. *N* is the number of simulation events. When *NRMSE* is < 1, the optimization works.

R can be expressed as follows:

$$R = \frac{1}{T}\sum_{t=1}^{T}\frac{\sum_{i=1}^{M}(sim_i^t - \overline{sim^t})\sum_{i=1}^{M}(obs_i^t - \overline{obs^t})}{\sqrt{\sum_{i=1}^{M}(sim_i^t - \overline{sim^t})^2}\sqrt{\sum_{i=1}^{M}(obs_i^t - \overline{obs^t})^2}}, \tag{5}$$

where $\overline{sim^t}$ and $\overline{obs^t}$ represent the average values of simulated and observed wind speed for all observation stations at time *t*. To obtain the total *R* value, the spatial *R* value at each time step is first evaluated, and then the *R* values of all time steps are averaged.

Generally, wind-speed frequency follows a Weibull distribution (Mathew, 2006), which is a probability density function (PDF) with a single peak and two parameters. The Weibull distribution is used to describe the overall wind-speed distribution. Its PDF can be expressed as follows:

$$f(v) = \frac{k}{c}\left(\frac{v}{c}\right)^{k-1}\exp\left[-\left(\frac{v}{c}\right)^k\right], (k > 0, v > 0), \tag{6}$$

where *v* is the wind speed (units: m s^{-1}); *k* and *c* are the two parameters; *k* is a shape parameter (dimensionless) that determines the basic shape of the PDF curve; *c* is a scale parameter (units: m s^{-1}) that can widen or narrow the curve as its value varies. The parameters *k* and *c* can be estimated using the average and standard deviation of wind speed. The corresponding expressions are:

$$k = \left(\frac{\sigma}{\bar{v}}\right)^{-1.086}, (1 \le k \le 10), \tag{7}$$

and

$$c = \frac{\bar{v}}{\left(0.568 + \frac{0.434}{k}\right)^{\frac{1}{k}}} \tag{8}$$

where σ is the standard deviation of wind speed and $\bar{v}$ is the average wind speed.

WPD is a more effective index than wind speed to express potential wind energy. It combines the comprehensive effect of wind speed and air density. The definition of WPD (units: W m^{-2}) is the mean power available when wind passes through one square meter of swept area of a turbine. The calculation formula for average WPD can be approximately expressed as follows:

$$WPD = \frac{1}{2n}\sum_{i=1}^{n}\rho v_i^3, \tag{9}$$

where *n* is the total number of wind energy records, v_i is the wind speed (units: m s^{-1}) for the *i*th record, and ρ is the air density (units: kg m^{-3}), which can be expressed as a function of altitude (*z*, units: m) and time-varying near-surface temperature (*T*, units: K) at the observation station. The formula is:

$$\rho = (353.05/T)\exp(-0.034(z/T)). \tag{10}$$

4. Results and discussion

4.1. Parameter SA results

The 270 perturbed parameter values in the twenty-seven-dimensional tunable parameter space are obtained by the GLP uniform sampling method. Each of the input perturbed parameters is respectively substituted into the WRF model to replace the default parameters, and the variation of hourly turbine-height wind speed is simulated in sixteen 3-day events [marked (1)–(16)] from June 2014 to May 2015, as shown in Fig. 2. The simulated hourly wind-speed errors are evaluated by the *RMSE* metric of the WRF simulations with default and perturbed parameters. As the inputs of the MARS SA method, the perturbed parameter values and the corresponding simulated hourly turbine-height wind-speed errors are entered into the MARS SA method, and the sensitivity scores of parameters for turbine-height wind-speed simulation are finally obtained. The parametric SA results are shown in Fig. 3. Seven sensitive parameters have been screened by the MARS SA method. Note that the scores of the

insensitive parameters are zero. The reason for this is that 100 MARS SA experiments are conducted, with the samples of each experiment obtained by bootstrapping for 270 sample sets. The final parameter sensitivity scores are obtained by averaging their SA scores in the 100 experiments. Therefore, the scores for the insensitive parameters are likely to become zero. Table 1 lists the seven screened sensitivity parameters from the six physical schemes.

Due to length constraints, further details of the parameter SA results are not discussed in this paper. The aim of this paper is mainly to demonstrate the effectiveness and efficiency of the ASMO parameter optimization method for improving WRF turbine-height wind simulation and for assessing the applicability of the optimal parameter values obtained.

4.2. Optimization efficiency analysis

The ASMO method is used in this study to estimate the seven WRF sensitive parameter values to improve turbine-height wind-speed simulation. The simulation period and the initial sampling method are the same as in the previous parameter SA experiments. However, the objective functions (i.e., the simulated errors) for the optimization is the *RMSE* metric of simulated hourly turbine-height wind speed between WRF simulations and observations. To demonstrate optimization efficiency more effectively, the *NRMSE* between simulated and observed hourly turbine-height wind speed is used. The number of initial sample points before the ASMO method is set to 100, and the samples are obtained using the GLP method. Based on the time requirements for computing 16 event simulations using the WRF model, the optimization criterion is designed as the local optimal value remaining unchanged after the number of search steps is equal to five times the parameter dimensionality.

Fig. 4 shows the convergence results for the WRF model adaptive parameter optimization for hourly turbine-height wind speed using the ASMO method. The simulation error is improved by ~5% using 100 initial sampling points, and the error is further decreased to 8.7% by adding another 31 sampling points using the adaptive optimization

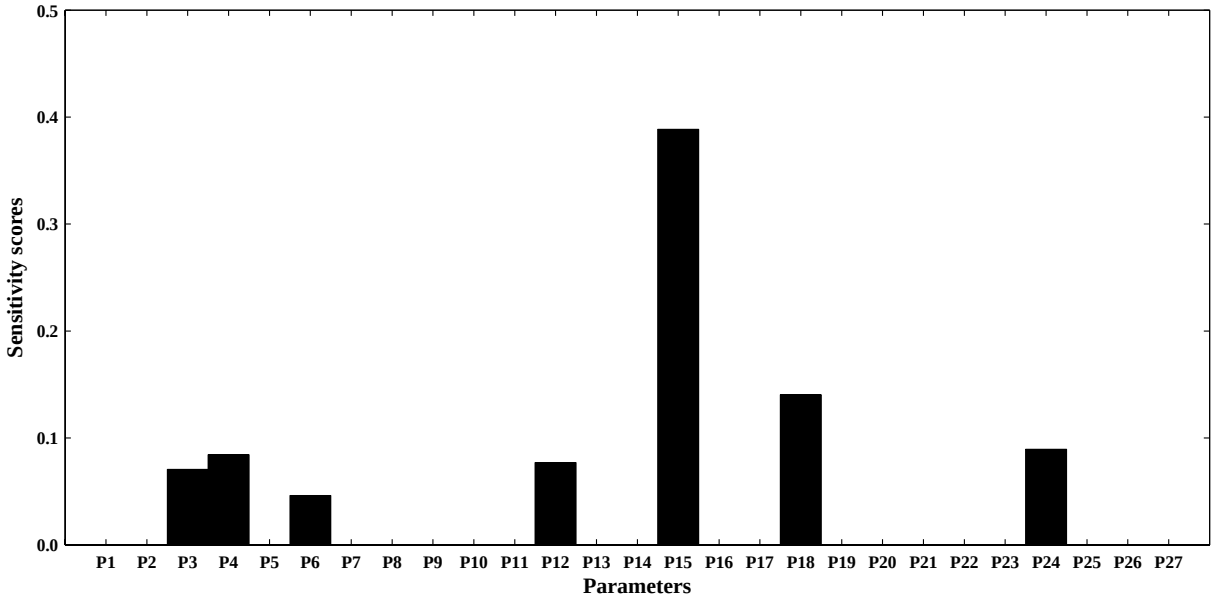

Fig. 3. Sensitivity scores of the twenty-seven tunable parameters.

strategy of the ASMO method. For hourly turbine-height wind-speed simulation, an improvement of 8.7% is highly significant. After 131 parameter samples, the optimal values of the seven WRF parameters affecting the simulation of turbine-height wind speed are finally found, demonstrating that the ASMO method is highly effective and efficient for parameter optimization of a complex dynamic model.

4.3. Analysis of optimization results

After the optimal parameter values are obtained from 131 parameter samples using the ASMO method, simulations of the sixteen 3-day events [(1)–(16)] using default and optimal parameters are compared; Fig. 5 shows the corresponding results. It is apparent that the overall simulation is improved by 8.7% and that the greatest improvement occurs for the simulation of event (4). It is also found that the optimal parameters evidently improve the turbine-height wind-speed simulations of most of the 16 events compared with the default parameters, except for the negative improvement (−0.06%) for event (2). The reason for this is that the defined objective function considers the average value of equal-weight *NRMSEs* for simulations of all 16 events. A few simulations with negative improvement are therefore unavoidable, although the overall simulation is greatly improved. If a suite of suitable unequal weights were allocated to the simulation error of each single event in the total objective function, it would be possible to improve both the simulation of each event and the overall simulation.

The 72-h variations of observed and simulated turbine-height wind speed are obtained by averaging the observations and simulations of the 16 events [(1)–(16)]. Fig. 6a shows the results. It is apparent that the WRF simulation with default parameters overestimates wind speed, but

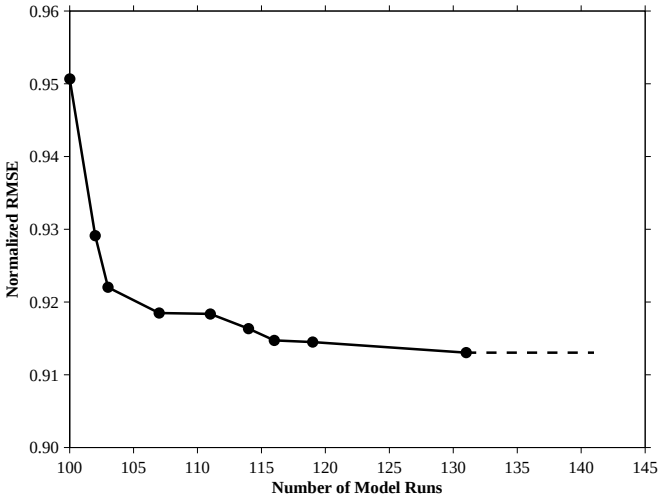

Fig. 4. Convergence results for the WRF model adaptive parameter optimization for hourly turbine-height wind speed using the ASMO method.

that the WRF simulation with optimized parameters significantly reduces the overestimation trend. The curve of the optimized simulation results is closer to observations than that of the default simulation results. In particular, the optimization effect is highly significant for wind speeds $> 6.5\,m\,s^{-1}$, and the maximum improvement occurs in the simulation of the strongest wind speed. For wind speeds $< 6.5\,m\,s^{-1}$, the optimization decreases the simulation errors, but a large bias remains between the observations and the default simulation, making its

Table 1
List of sensitivity parameters from six physical schemes for WRF model version 3.7.1.

Index	Parameter	Scheme	Default	Range	Description
P3	surface_1	Surface layer (module_sf_sfclayrev.F)	1	[1, 2]	Scaling related to surface roughness
P4	karman		0.4	[0.35, 0.4]	Von Kármán constant
P6	convection_2	Cumulus (module_cu_kfeta.F)	1	[0.5, 1.5]	Scaling related to entrainment flow
P12	microphys_2	Microphysics (module_mp_gsfcgce.F)	3.29	[1.65, 4.94]	Scaling related to ice fall terminal velocity(s^{-1})
P15	radiation_2	Short wave radiation (module_ra_rrtmg_sw.F)	1	[0.5, 1.0]	Scaling related to cloud single scattering
P18	land_2	Land surface (module_sf_noahlsm.F)	1	[0.5, 1.5]	Scaling related to soil porosity
P24	planetary_3	Planetary boundary layer (module_bl_ysu.F)	2	[1, 3]	Profile shape exponent of the momentum diffusivity

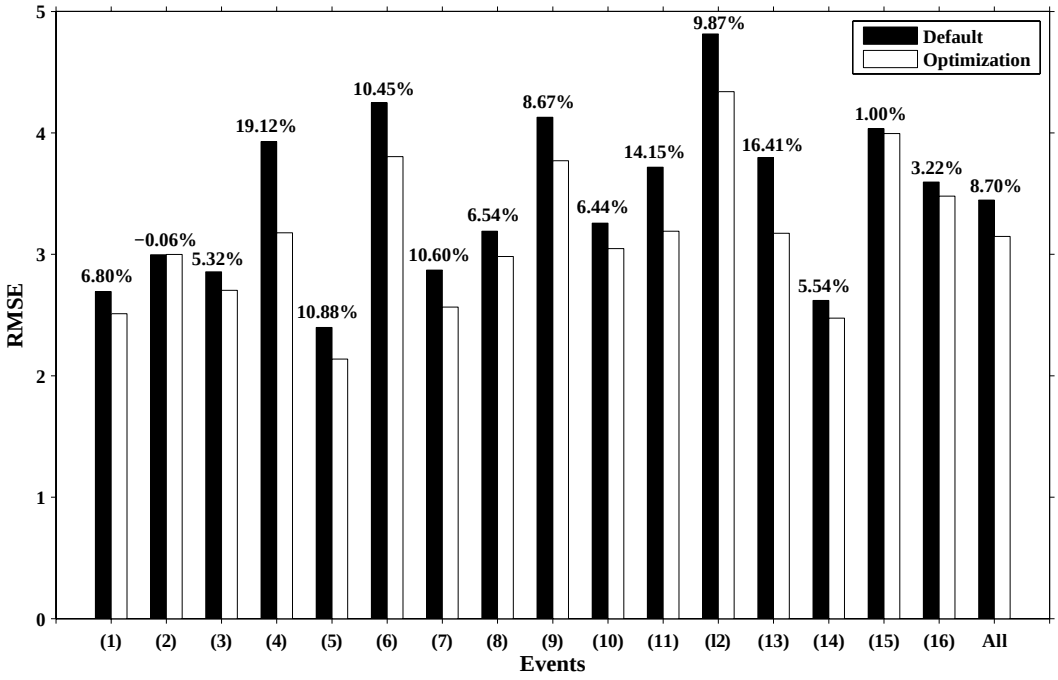

Fig. 5. Comparison of wind-speed simulation errors for sixteen events (1)–(16) using the WRF model with default and optimal parameters.

improvement effect weaker than that when wind speeds > 6.5 m s^{-1}.

In addition, it has been demonstrated that WRF model simulations can better capture the daily variation characteristics of turbine-height wind speed. By converting Universal Time Coordinates (UTC) into local time (i.e., Beijing time), it is found that the wind speed is lower in the daytime and higher at night. More specifically, the lowest wind speed occurs at ~ 14:00 local time (corresponding to 6:00, 30:00, and 54:00 in UTC, as shown in Fig. 6a), whereas the wind speed at local night time (corresponding to 12:00–24:00, 36:00–48:00, and 60:00–72:00 in UTC, as shown in Fig. 6a) is relatively strong and steady. Overall, the reasonable simulation results prove the suitability of the WRF model to simulate turbine-height wind speed, and the significant improvement of

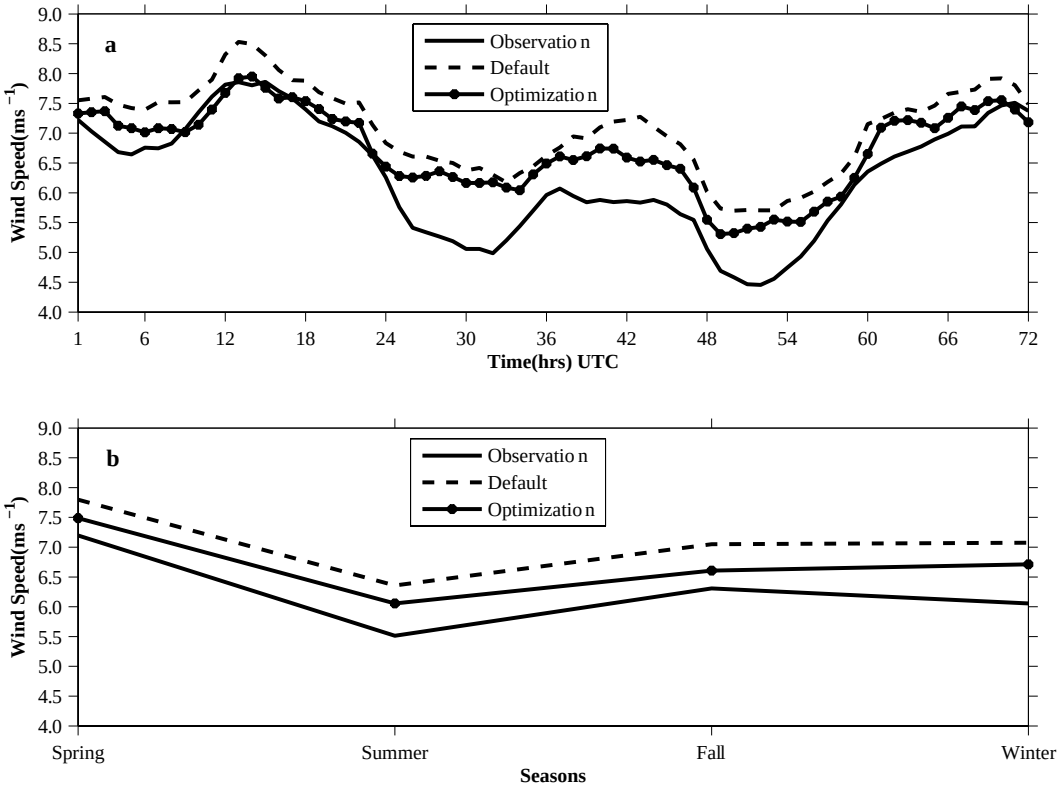

Fig. 6. Comparisons of time variations in observed and simulated turbine-height wind speed using the WRF model with default and optimal parameters for: (a) 72-h lead times (b) four seasons.

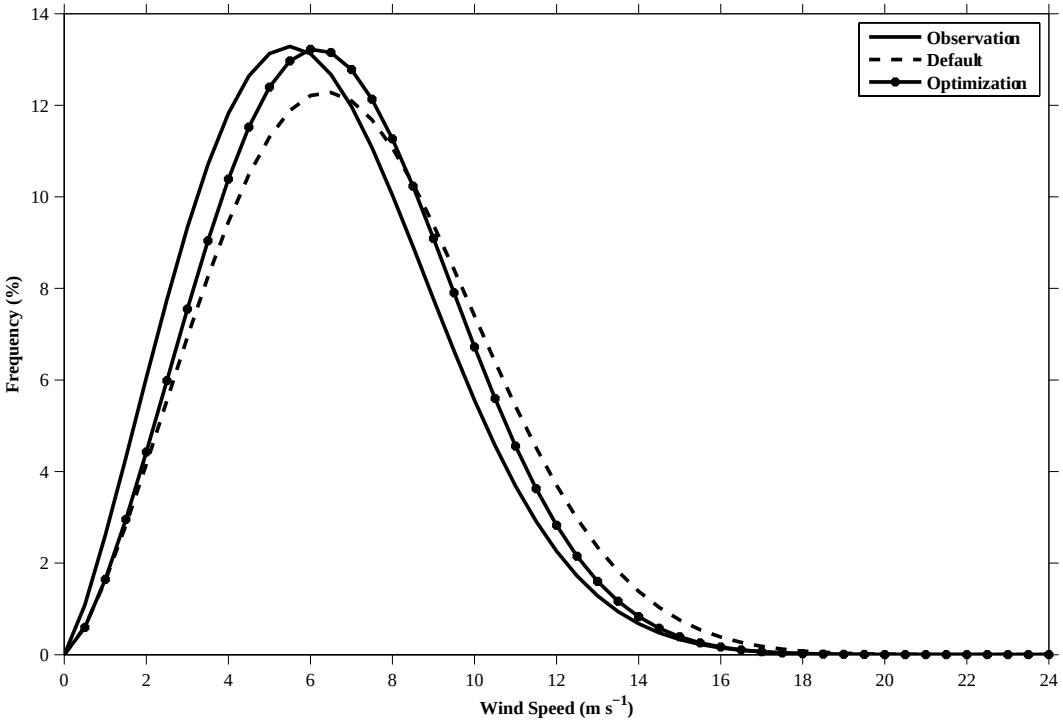

Fig. 7. Comparison of the Weibull PDFs of observed and simulated turbine-height wind speed.

the hourly simulations demonstrates the effectiveness of the ASMO parameter optimization method.

Because the 16 optimization events [(1)–(16)] are chosen from the four seasons of one year (i.e., from June 2014 to May 2015), the comparisons of optimized and default simulations are conducted for the four seasons. Specifically, events (1)–(4), (5)–(8), (9)–(12), and (13)–(16) belonged to summer, fall, winter, and spring respectively. Fig. 6b shows the comparison results for observed and simulated turbine-height wind speed with default and optimal parameters for the four seasons. Compared to observations, the simulations with both default and optimal parameters have the consistent variance characteristic that turbine-height wind speed is highest in spring and lowest in summer. It is also apparent that the optimal parameters greatly improve the turbine-height wind-speed simulations for the four seasons compared to the default parameters. The improvement rates in spring and fall with strong wind are obviously higher than those in summer and winter with light wind, which confirms once more that the ASMO method achieves significant improvement for the simulation of strong wind (see Fig. 6a).

Fig. 7 shows the Weibull PDFs of observed and simulated turbine-height wind speed. When comparing the median values of the Weibull PDFs, it is found that the WRF simulations with default parameters overestimate wind speeds compared to the observed data and that the simulated values of average wind speed are closer to observations when ASMO parameter optimization is used. Similarly, the frequency of the simulated median wind speed is also brought closer to observations by parameter optimization. Comparing the whole set of Weibull PDFs for the observations and the simulation with default parameters, it is demonstrated that the simulation with default parameters strongly overestimates the frequency of strong winds with speeds $> 7\,\mathrm{m\,s^{-1}}$ and underestimate the frequency of light winds with speeds $< 7\,\mathrm{m\,s^{-1}}$. The overall result is that the simulated wind speed using the WRF model with default parameters overestimate the observations. The simulation with optimal parameters obtained by the ASMO method reduces the frequency of simulated strong winds and increases the frequency of simulated light winds, bringing the optimization results closer to observations.

The optimal parameters obtained by optimizing the turbine-height wind-speed simulations are also used to evaluate the effects on profile simulations of wind speed and temperature in the entire atmospheric layer (i.e., with pressure coordinates from 1000 to 100 hPa). The simulated variables (e.g., wind speed or temperature) are first interpolated into vertical pressure layers, and then the variable values for each pressure layer are horizontally interpolated to the locations of the four sounding observation points (marked as blue points in Fig. 1). According to measured data for the specific pressure layers at the sounding observation points, the *RMSE* of the 12-hourly simulated variables for each specific pressure layer is evaluated for the 16 events [(1)–(16)]. Finally, the profile errors of simulated wind speed and temperature are respectively obtained by averaging the profile errors of the corresponding variables at the four sounding observation points.

Fig. 8a shows a comparison of wind-speed profile errors for WRF simulations with default and optimal parameters. It is evident that the WRF model with optimal parameters improves the wind-speed simulations below the height with 250 hPa air pressure, but achieves a negative improvement for heights between 100 and 250 hPa. Similarly, Fig. 8b shows a comparison of temperature profile errors for WRF simulations with default and optimal parameters. Unlike the wind-speed profiles, the temperature profile simulations using the optimal parameters are distinctly improved in all pressure layers compared to the simulations with default parameters. Therefore, it can be said that the optimal parameters have a distinct ability to improve simulated wind-speed and temperature profiles in the entire atmospheric layer.

R is another common statistical metric for evaluating turbine-height wind-speed simulations. In this study, the optimal parameters obtained by optimizing the *RMSE* of hourly turbine-height wind-speed simulations are tested to examine whether they still can improve the *R* of the default WRF simulations. Fig. 9 shows a comparison of *R* for the WRF simulations with default and optimal parameters. Overall, the optimal parameters improve the *R* of the wind-speed simulations by approximately 4% compared to the default parameters. This means that the optimal parameters obtained by optimizing the *RMSE* of hourly turbine-height wind-speed simulations not only improve the *RMSE* of the wind-speed simulations by 8.7%, but also improve the *R* of the wind-speed

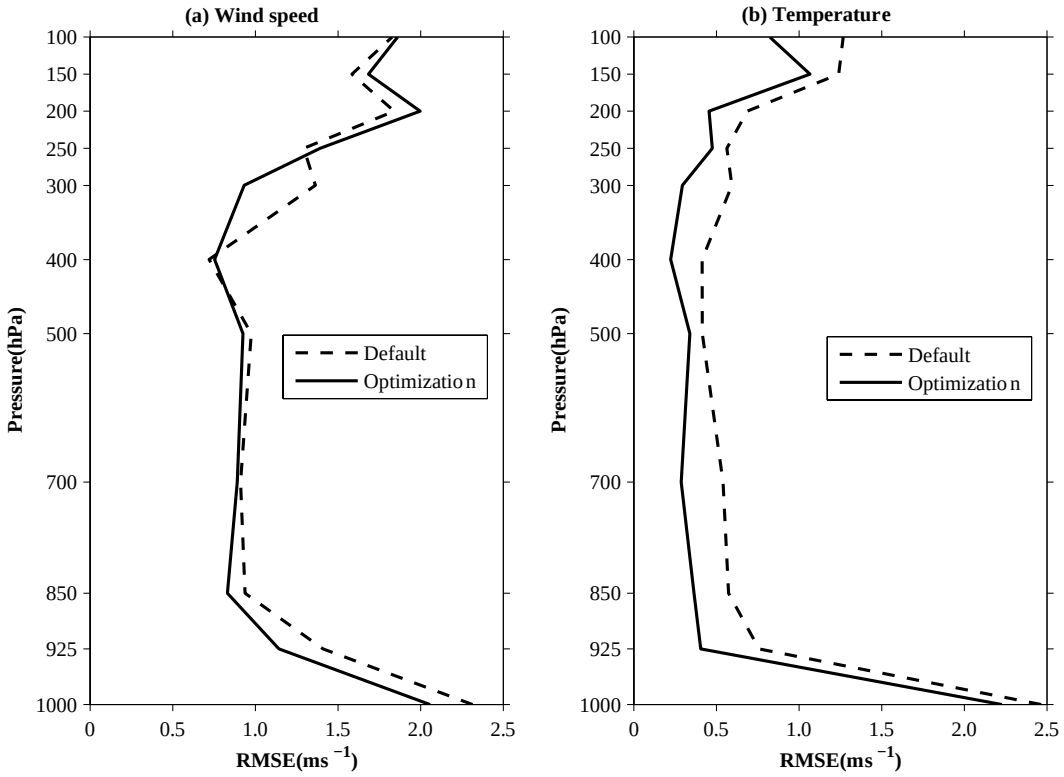

Fig. 8. Comparisons of profile simulation errors using WRF model with default and optimal parameters for: (a) wind speed (b) temperature.

simulations by approximately 4%. Obviously, the applicability of the WRF optimal parameters obtained using the ASMO method has been further demonstrated. Note that 14 of the 16 events show improvement in wind-speed simulation, but two events (2)–(3) do not. The reason for this is related to the definition of the objective function only using *RMSE*. If *R* is also added into the optimization objective function, the negative improvements will disappear.

4.4. WPD improvement analysis

WPD is a common metric to assess wind-energy potential. According to Eq. (9), WPD is proportional to the cube of turbine-height wind speed. Therefore, when the accuracy of simulated turbine-height wind speed has been improved, it is desirable to analyze the variation in WPD. As input data, the heights of the observation stations and the time-varying air temperatures at 10 m are substituted into Eq. (10) to

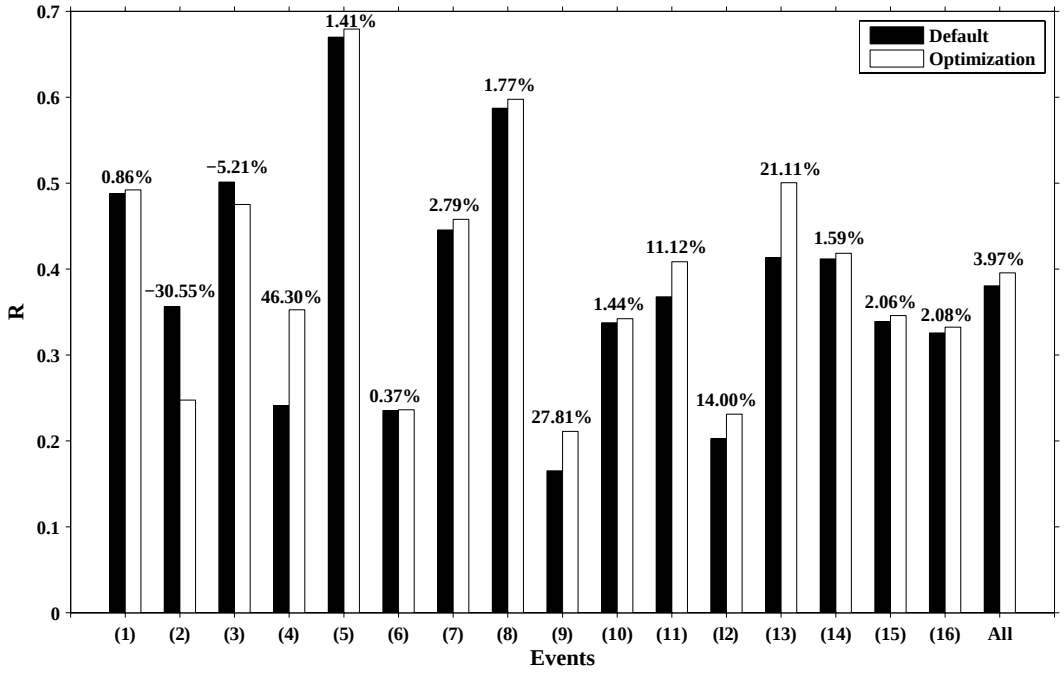

Fig. 9. Comparison of *R* for the WRF wind-speed simulations with default and optimal parameters.

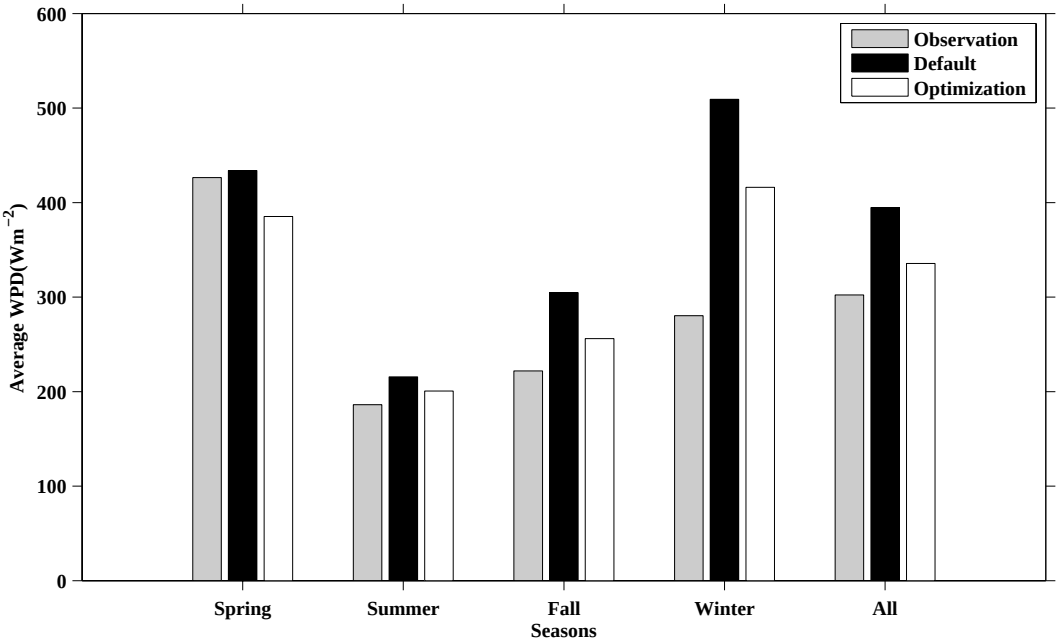

Fig. 10. Comparison of simulated and observed WPD values over the four seasons.

evaluate the time-varying air density values. Finally, WPD is evaluated as the product of air density and the cube of wind speed.

Based on the evident variations in turbine-height wind speed over the seasons (see Fig. 6b), an analysis of average WPD is conducted in each season. Fig. 10 shows a comparison of simulated and observed WPD for the four seasons and the whole year. The observed WPD values are obtained by evaluating Eq. (9)–Eq. (10) using observed air-temperature data at 10 m, turbine-height wind speed, and the heights of the observation stations. Fig. 10 illustrates that the WPD calculated using the optimal wind speed shows significant improvement and is closer to the corresponding observations for the whole year and the three seasons of summer, fall, and winter compared with the WPD calculated using the default wind speed. The improvement is especially significant for fall and winter. Moreover, the negative improvement of the optimization simulation in spring does not change the fact that the WRF simulation with optimal parameters improves WPD estimation by approximately 36% for the whole year compared to the WRF default simulation. In accordance with the distribution of average turbine-height wind speed in the four seasons (see Fig. 6b), the WPD is also highest in spring and lowest in summer, demonstrating that WPD variation is mainly affected by variation in turbine-height wind speed. Note also that the ranking of improvement rates for WPD is inconsistent with that of wind speed, which may be related to the variations in air density across the seasons.

To obtain a better assessment of the spatial distribution of wind energy, the spatial distribution of the simulated WPD with optimal wind speed is evaluated, and the results are shown in Fig. 11. It is clear that the strongest wind-energy resources are mainly distributed along the border between Henan and Hubei Provinces and that between Anhui and Hubei Provinces, where the terrain is mainly high mountains and the average WPD is $> 500\,W\,m^{-2}$. For the northern provinces, the average WPD ranges from 200 to $300\,W\,m^{-2}$. For the southern provinces, the average WPD ranges from 100 to $200\,W\,m^{-2}$. Fig. 11 also shows the positions of the observation stations marked with red asterisks. From the positions of the observation stations and the WPD spatial distribution, it is clear that most of the observation stations are built in the regions with high wind energy, but a few are built in regions with low wind energy (see the bottom right corner in Fig. 11). Therefore, from the viewpoint of wind-energy simulation, it can be concluded that the locations of some already-built observation stations are inappropriate.

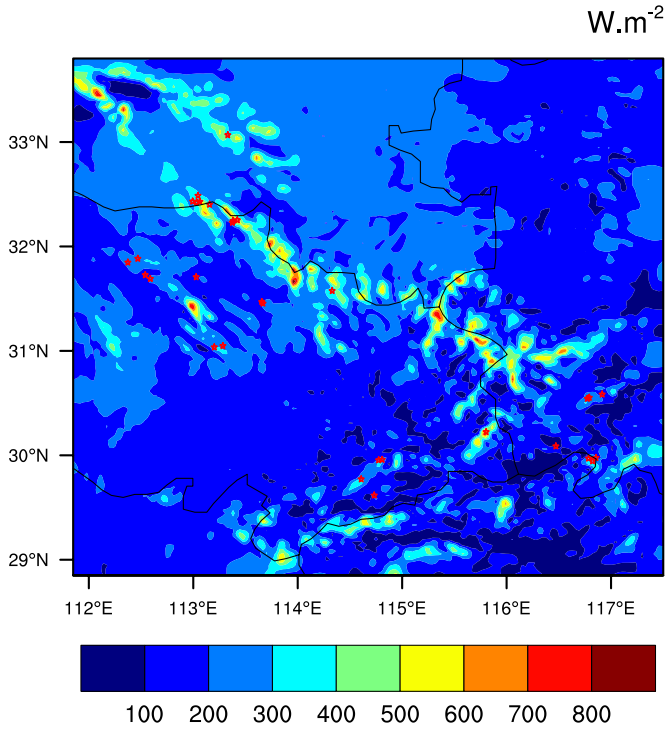

Fig. 11. Spatial distribution of simulated WPD with the optimal wind speed. The red asterisks represent the positions of the observation stations. (For interpretation of the references to colour in this figure legend, the reader is referred to the web version of this article.)

4.5. Validation analysis of WRF optimal parameters

Compared with the default parameters, the superiority of the optimal parameters obtained by the ASMO method for improving WRF turbine-height wind-speed simulation has been demonstrated in the optimization period. However, for the validation period when new

Table 2
The six validation events from June 2014 to May 2015.

Events	Duration
I	2014/09/26–2014/09/28
II	2014/09/29–2014/10/01
III	2014/12/28–2014/12/30
IV	2014/12/31–2015/01/02
V	2015/03/14–2015/03/16
VI	2015/03/17–2015/03/19

events must be simulated, the question whether the optimal parameters are still effective deserves to be investigated. Six new validation events are selected from June 2014 to May 2015, as shown in Table 2. The designs of the domain and simulation, the variation characteristics of wind speed and direction, the simulation duration, and the forcing data source are the same as in the parameter optimization experiment.

Fig. 12a compares the *RMSE* of simulated hourly turbine-height wind speed using the WRF model with default and optimal parameters for the six validation events. Overall, compared with the WRF simulations with default parameters, the average improvement percentage of *RMSE* in the WRF wind-speed simulations is 7.58% using WRF simulations with optimal parameters. Moreover, all validation event simulations are improved using the WRF simulations with optimal parameters, and the wind-speed simulations are improved by percentages varying from 2.63% to 12.29%. Fig. 12b shows a comparison of *R* for the simulated hourly turbine-height wind speed using the WRF model with default and optimal parameters. Overall, the average improvement percentage of *R* in the WRF wind-speed simulations with optimal parameters is 6.49%, demonstrating that the optimal parameters can also improve the correlation of WRF turbine-height wind-speed simulations in the validation events. Note that one of the six single-objective simulations experiences negative improvement, which may be related to the parameter values obtained by optimizing *RMSE*.

Note that the observed wind evolution for the calibration and validation periods follows two pattern variations: one is that when the wind speed increases (light to strong), the wind direction experiences a south-to-north variation, and the other is that when the wind speed decreases (strong to light), the wind direction experiences a north-to-south variation. However, it is unknown whether the optimal parameters still work when other wind patterns are simulated. In this section, two opposite wind patterns are selected for simulation to validate further the superiority of the optimal parameters. Each pattern includes three 3-day wind events. Fig. 13a–c shows the first pattern, in which when wind speed decreases (strong to light), the wind direction variation is approximately south-to-north; Fig. 13d–f shows the second pattern, in which when wind speed increases (light to strong), the wind direction variation is approximately north-to-south. Fig. 13a–f illustrates the new events (A)-(F), respectively.

The two categories of simulations are separately compared to examine whether the optimal parameters work for simulations of other wind patterns. Fig. 14 shows the comparison results. It is apparent that the optimal parameters improve the simulations of all six wind events compared with the default parameters. Overall, using WRF simulations with optimal parameters, the average improvement percentages in *RMSE* in hourly turbine-height wind-speed simulation for the two newly simulated wind patterns are 6.68% and 4.66%, respectively. This demonstrates that the optimal parameters are reasonable for simulating different wind patterns, and the method is therefore effective in improving WRF turbine-height wind-speed simulation.

Overall, the optimal parameters obtained by optimizing the *RMSE* of turbine-height wind-speed simulations using the ASMO method not only improve the *R* of wind-speed simulations in the optimization period, but also improve the *RMSE* and *R* of wind-speed simulations in the validation period. In addition, the optimal parameters can be used to simulate other wind patterns. These analyses demonstrate comprehensively that the optimal parameters can be used to improve turbine-height wind-speed simulations in the study area. Therefore, the optimal parameter values are thought to be reasonable and effective.

4.6. Physical interpretation and verification of the optimal parameter values

The values of the default and optimal parameters are normalized within their ranges to provide a clearer illustrate of the variations between them. Fig. 15 shows a comparison of the normalized optimal and default parameter values. All the optimal parameter values show

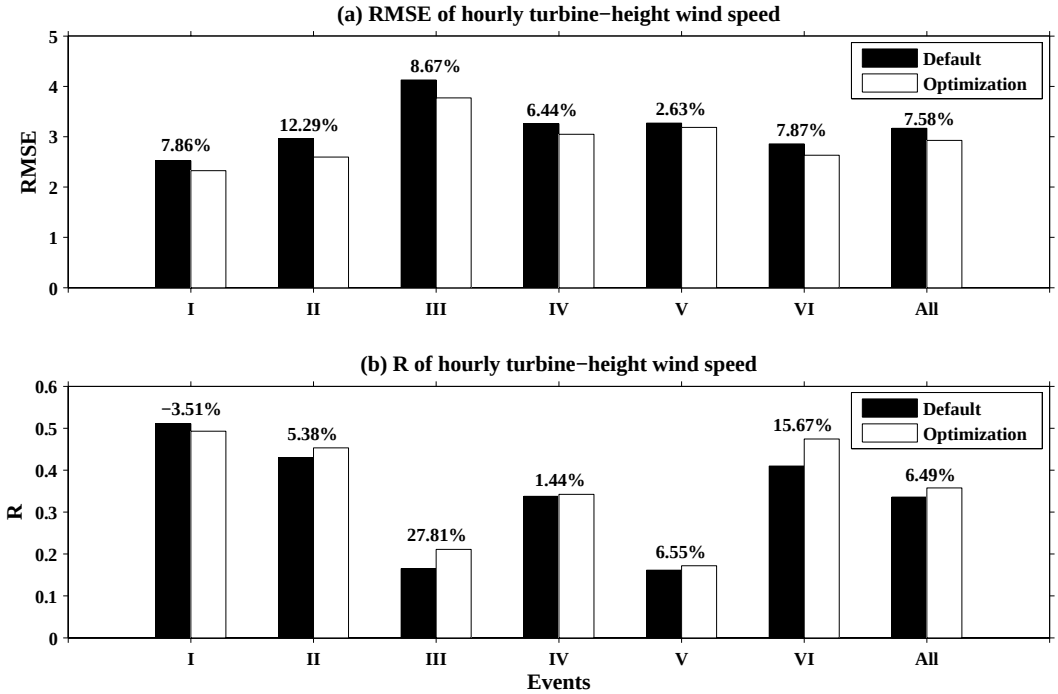

Fig. 12. Comparisons of simulation errors of hourly turbine-height wind speed using WRF model with default and optimal parameters for: (a) *RMSE* (b) *R*.

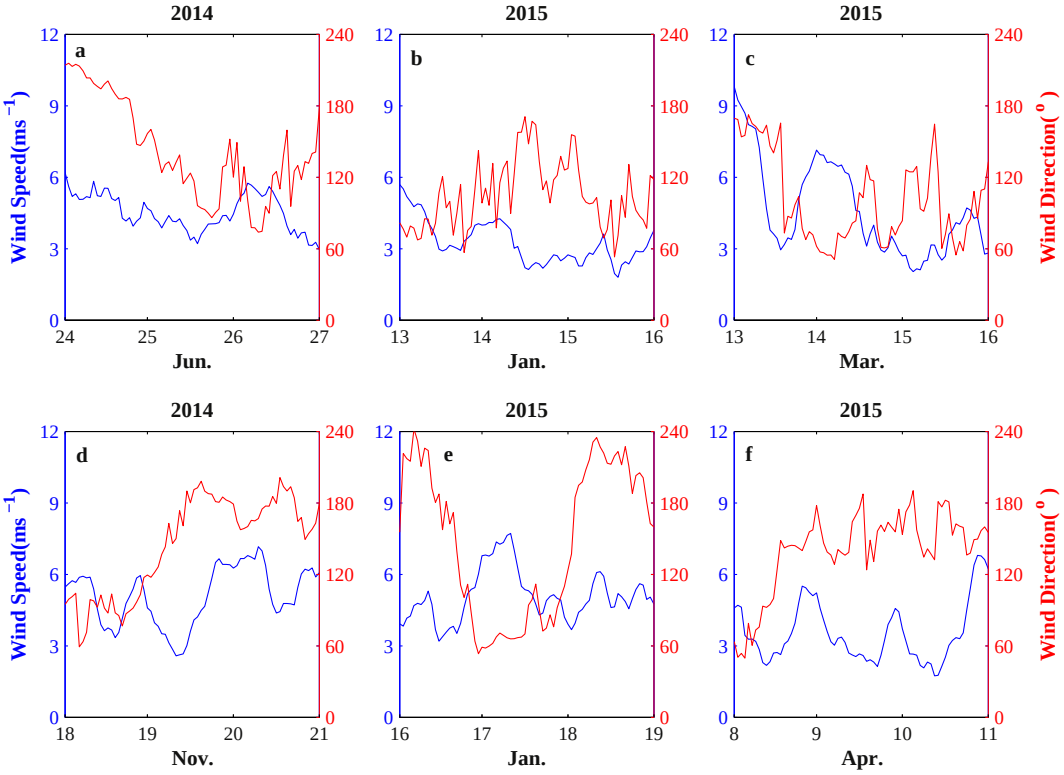

Fig. 13. Two different wind patterns. (a)-(c) is the first category, in which the wind speed gradually decreases and the wind direction experiences an approximately south-to-north variation; (d)-(f) is the second category, in which the wind speed gradually increases and the wind direction experiences an approximately north-south variation.

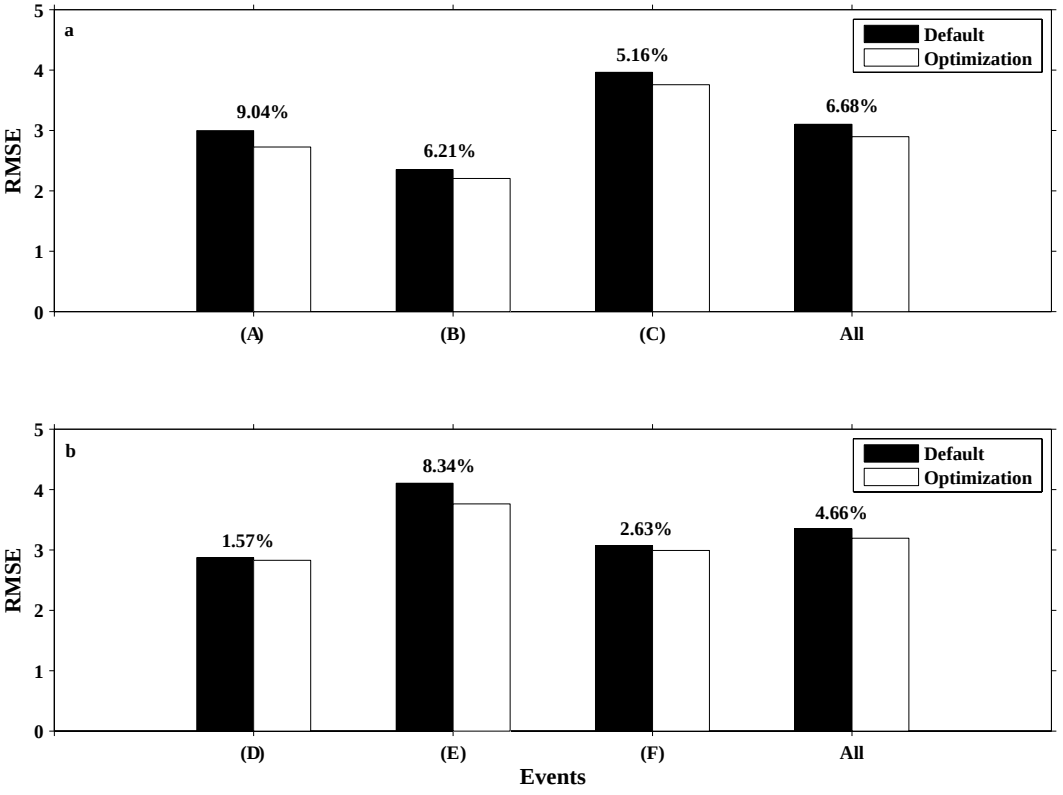

Fig. 14. Comparisons of simulation errors in hourly turbine-height wind speed using the WRF model with default and optimal parameters for: (a) the wind pattern with wind speed decreasing and wind direction changing south-to-north (b) the wind pattern with wind speed increasing and wind direction changing north-to-south.

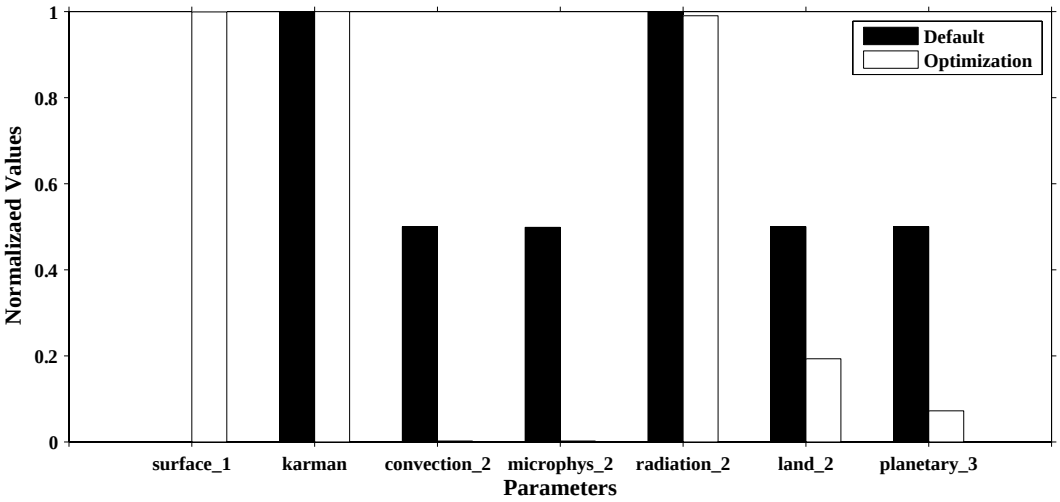

Fig. 15. Comparison of the normalized optimal and default parameter values.

inconsistent variations. For the *karman* (the von Kármán constant) and *radiation_2* (scaling related to aerosol single scattering) parameters, their values are basically unchanged and remained the same as the default parameter values. For the *surface_1* (scaling related to surface roughness) parameter, the value varies from the minimum for the default parameter to the maximum for the optimal parameter in its range. For the other four parameters, their optimal values are lower than their default values.

It has been found from previous analyses (e.g., Fig. 6) that the default simulation parameters generally overestimate wind-speed values compared with observations and that the optimal simulation parameters reduce this overestimation. The specific physical interpretation of the parameter variation is the following. Larger values of *surface_1* mean a greater roughness length to be defined in the surface layer, which elevates the zero-plane displacement height and therefore reduces wind speed at turbine height. Larger values of *karman* enhance the magnitude of the turbulent length scale in the planetary boundary layer, leading to stronger vertical mixing during daytime. However, larger values of *karman* also lead to increases in the exchange coefficient for momentum near surface, causing a reduction of wind speed. Smaller values of *convection_2* (scaling related to entrainment flow) lead to lower ratios of entrainment to updraft flux, which enhances the updraft, leading to decreases in horizontal wind speeds. The *microphys_2* parameter (scaling related to ice fall) directly affects the conversion rate from cloud ice to rainwater in the description of the microphysics parameterization scheme. Therefore, smaller values of *microphys_2* eventually brings about reductions in precipitation, leading to decreases in evapotranspiration or turbulence and reductions in turbine-height wind speed. Larger values of *radiation_2* lead to more scattering of solar radiation reflected to the sky, which reduces the amount of shortwave radiation reaching the surface, further suppressing evaporation and ultimately leading to decreases in wind speeds. Small values of *land_2* (scaling related to soil porosity) lead to lower soil porosity, which suppresses the conveyance of soil water and heat upward from groundwater to the surface and thus decreases the difference between surface energies at different locations, blocking the development of wind speed. The *planetary_3* parameter (profile shape exponent of the momentum diffusivity) has a positive effect on the momentum diffusivity coefficient. When *planetary_3* decreases, the eddy turbulence diffusivity intensity is weakened, inducing lower wind speed at turbine height.

5. Conclusions

This study first uses the global SA method to identify the seven sensitive parameters from 27 tunable parameters in seven WRF physical parameterization schemes and then optimizes the seven sensitivity parameters from the six WRF physical parameterization schemes using the ASMO method to improve turbine-height wind-speed simulation over Eastern China. The WRF model simulations with default and optimal parameters are compared from five aspects, including the variation of turbine-height wind speed over a 72-h lead time and the four seasons, the Weibull frequency distribution of wind speed, wind-speed and temperature profiles from 1000 to 100 hPa, the correlation of simulated wind speed, and the spatial and temporal distribution of WPD in the study area. In addition, the applicability of the optimal parameters obtained by the ASMO method is examined in new simulations of the six validation events to show their superiorities to the default parameters for improving turbine-height wind-speed simulation.

The optimization results demonstrate that parameter optimization for the complex WRF model, which has very time-consuming calculation requirements, can be conducted using the ASMO method. In particular, the optimal values of the seven parameters in this study are obtained using 131 samples, including 100 initial and 31 adaptive samples obtained using the ASMO method. This approach greatly reduces the number of WRF model runs and demonstrates that the ASMO method is a highly effective and efficient optimization method and is well suited to optimize the parameters of other complex weather and climate models.

By comparing the WRF model simulations with default and optimal parameters, it is found that the hourly turbine-height wind-speed simulation is improved by 8.7% using ASMO optimization. Variation analyses of wind-speed time series show that the WRF simulation with default parameters overestimates wind speed, whereas the WRF simulation with optimized parameters greatly reduces the overestimation trend. By comparing the simulated Weibull frequency distributions, it has been found that the WRF model with optimal parameters reduces the frequency of simulated strong winds and increases the frequency of simulated light winds, bringing the optimization results closer to observations. Besides improving turbine-height wind-speed simulation, the WRF model with optimal parameters also improves the simulation of wind and temperature profiles from 1000 to 100 hPa. Similarly, it also improves the R of turbine-height wind-speed simulation by approximately 4% in addition to improving *RMSE* by 8.7% as the cost function. Based on the WPD formula, it has been demonstrated that the WRF model with optimal parameters improves WPD estimation by 36%. By examining the spatial distribution of WPD simulations with optimal wind speeds, it has also been found that the locations of a few observation stations built in regions with low wind energy are inappropriate, although most of the stations are built in high-wind-energy

regions. Finally, the applicability of the optimal parameters is also demonstrated by comparing turbine-height wind-speed simulations for two categories of new validation events: one is the same pattern as the calibration events, whereas the other represents an opposite pattern. The results show that the WRF model with optimal parameters improves the *RMSE* and *R* of wind speed simulations for the same pattern of six validation events by 7.58% and 6.49% respectively. For the two different patterns, the average *RMSE* improvement percentages of wind-speed simulations for the three valiation events are 6.68% and 4.66%, respectively. This fully demonstrates the reasonableness of the optimal parameters.

However, it should be noted that generally the wind-speed simulations are improved by the WRF model with optimal parameters, but that several single simulations show negative improvements. These phenomena are caused by the definition of the single-objective cost function, which allocates equal weight to each single simulation and then averages all the simulation errors. If the suitable weights are used to construct the multi-objective cost function, it will be possible to improve all the single simulations using multi-objective optimization methods such as NSGA-II (Deb et al., 2002) and ASMO-PODE (Gong and Duan, 2017). In addition, the same approach can be migrated to other multi-variable joint optimization problems such as wind speed, temperature, and pressure.

Acknowledgements

This research was supported by the Ministry of Science and Technology of China (No. IUMKY201603), the Strategic Priority Research Program of the Chinese Academy of Sciences (Nos. XDA19070104, XDA20060401), the Intergovernmental Key International S&T Innovation Cooperation Program (No. 2016YFE0102400), the Special Fund for Meteorological Scientific Research in the Public Interest (No. GYHY201506002, CRA–40: 40-year CMA global atmospheric reanalysis), the National Basic Research Program of China (No. 2015CB953703), and the Natural Science Foundation of China (41305052). We acknowledge National Center for Environmental Prediction Reanalysis dataset (http://rda.ucar.edu/datasets/ds083.2/) and sounding dataset (http://weather.uwyo.edu/upperair/sounding.html). The hourly turbine-height wind-speed dataset are avail upon request from the author Dr. Ao.

Appendix A. Supplementary data

Supplementary data to this article can be found online at https://doi.org/10.1016/j.atmosres.2019.04.011.

References

Avolio, E., Federico, S., Miglietta, M.M., Feudo, T.L., Calidonna, C.R., Sempreviva, A.M., 2017. Sensitivity analysis of WRF model PBL schemes in simulating boundary-layer variables in southern Italy: an experimental campaign. Atmos. Res. 192, 58–71. https://doi.org/10.1016/j.atmosres.2017.04.003.

Boffey, P.M., 1970. Energy crisis: environmental issue exacerbates power supply problem. Science 168, 1554–1559. https://doi.org/10.1126/science.168.3939.1554.

Bossanyi, E.A., 1985. Short-term wind prediction using Kalman filters. Wind Eng. 9, 1–8.

Chen, F., Dudhia, J., 2001. Coupling an advanced land surface–hydrology model with the Penn State–NCAR MM5 modeling system part I: model implementation and sensitivity. Mon. Weather Rev. 129, 569–585. https://doi.org/10.1175/1520-0493(2001)129<0569:CAALSH>2.0.CO;2.

Deb, K., Pratap, A., Agarwal, S., Meyarivan, T., 2002. A fast and elitist multiobjective genetic algorithm: NSGA-II. IEEE T. Evolut. Comput. 6, 182–197. https://doi.org/10.1109/4235.996017.

Deppe, A., Gallus, W., Takle, E., 2013. A WRF ensemble for improved wind speed forecasts at turbine height. Weather Forecast. 28, 212–228. https://doi.org/10.1175/WAF-D-11-00112.1.

Di, Z., Duan, Q., Gong, W., Wang, C., Gan, Y., Quan, J., Li, J., Miao, C., Ye, A., Tong, C., 2015. Assessing WRF model parameter sensitivity: a case study with 5 day summer precipitation forecasting in the Greater Beijing Area. Geophys. Res. Lett. 42, 579–587. https://doi.org/10.1002/2014GL061623.

Di, Z., Duan, Q., Gong, W., Ye, A., Miao, C., 2017. Parametric sensitivity analysis of precipitation and temperature based on multi-uncertainty quantification methods in the weather research and forecasting model. Sci. China Earth Sci. 60, 876–898. https://doi.org/10.1007/s11430-016-9021-6.

Di, Z., Duan, Q., Wang, C., Ye, A., Miao, C., Gong, W., 2018. Assessing the applicability of WRF optimal parameters under the different precipitation simulations in the Greater Beijing Area. Clim. Dyn. 50, 1927–1948. https://doi.org/10.1007/s00382-017-3729-3.

Duan, Q., Sorooshian, S., Gupta, V.K., 1994. Optimal use of the SCE-UA global optimization method for calibrating watershed models. J. Hydrol. 158, 265–284. https://doi.org/10.1016/0022-1694(94)90057-4.

Duan, Q., Di, Z., Quan, J., Wang, C., Gong, W., Gan, Y., Ye, A., Miao, C., Miao, S., Liang, X., Fan, S., 2017. Automatic model calibration: a new way to improve numerical weather forecasting. B. Am. Meteorol. Soc. 98, 959–970. https://doi.org/10.1175/BAMS-D-15-00104.1.

Dudhia, J., 2014. A history of mesoscale model development. Asia-Pac. J. Atmos. Sci. 50, 121–131. https://doi.org/10.1007/s13143-014-0031-8.

Dudhia, J., Gill, D., Manning, K., Wang, W., Bruyere, C., 1999. PSU/NCAR Mesoscale Modeling System Tutorial Class Notes and user's Guide: MM5 Modeling System Version 3. (Boulder).

Dvorak, M., Archer, C., Jacobson, M., 2010. California offshore wind energy potential. Renew. Energy 35, 1244–1254. https://doi.org/10.1016/j.renene.2009.11.022.

Fan, X., Krieger, J., Zhang, J., Zhang, X., 2013. Assimilating quikSCAT ocean surface winds with the Weather Research and forecasting model for surface wind-field simulation over the Chukchi/Beaufort seas. Bound.-Layer Meteorol. 148, 207–226. https://doi.org/10.1007/s10546-013-9805-2.

Fernández-González, S., Martín, M.L., Garcrc-Ortega, E., Merino, A., Lorenzana, J., Sánchez, J.L., Valero, F., Rodrigo, J.S., 2018. Sensitivity analysis of WRF model: wind-resource assessment for complex terrain. J. Appl. Meteorol. Climatol. 57, 733–753. https://doi.org/JAMC-D-17-0121.1.

Fernández-González, S., Sastre, M., Valero, F., Merino, A., García-Ortega, E., Sánchez, J., Lorenzana, J., Martín, M., 2019. Characterization of spread in a mesoscale ensemble prediction system: Multiphysics versus initial conditions. Meteorol. Z. 28, 59–67. https://doi.org/10.1127/metz/2018/0918.

Friedman, J., 1991. Multivariate adaptive regression splines. Ann. Stat. 19, 1–141. https://doi.org/10.1214/aos/1176347963.

Gong, W., Duan, Q., 2017. An adaptive surrogate modeling-based sampling strategy for parameter optimization and distribution estimation (ASMO-PODE). Environ. Model. Softw. 95, 61–75. https://doi.org/10.1016/j.envsoft.2017.05.005.

Gong, W., Duan, Q., Li, J., Wang, C., Di, Z., Dai, Y., Ye, A., Miao, C., 2015. Multi-objective parameter optimization of common land model using adaptive surrogate modeling. Hydrol. Earth Syst. Sc. 19, 2409–2425. https://doi.org/10.5194/hess-19-2409-2015.

Gong, W., Duan, Q., Li, J., Wang, C., Di, Z., Ye, A., Miao, C., Dai, Y., 2016. An intercomparison of sampling methods for uncertainty quantification of environmental dynamic models. J. Environ. Inf. 28, 11–24. https://doi.org/10.3808/jei.201500310.

Grubb, M., Meyer, N., 1993. Wind Energy: Resources, Systems and Regional Strategies, in Renewable Energy. Island press, Washington, pp. 157–212.

Hahmann, A., Vincent, C., Pena, A., Lange, J., Hasager, C., 2015. Wind climate estimation using WRF model output: method and model sensitivities over the sea. Int. J. Climatol. 35, 3422–3439. https://doi.org/10.1002/joc.4217.

Hariprasad, K.B.R.R., Srinivas, C.V., Singh, A.B., Rao, S.V.B., Baskaran, R., Venkatraman, B., 2014. Numerical simulation and intercomparison of boundary layer structure with different PBL schemes in WRF using experimental observations at a tropical site. Atmos. Res. 145–146, 27–44. https://doi.org/10.1016/j.atmosres.2014.03.023.

Holman, B.P., Lazarus, S.M., Splitt, M.E., 2018. Statistically and dynamically downscaled, calibrated, probabilistic 10-m wind vector forecasts using ensemble model output statistics. Mon. Weather Rev. 146, 2859–2880. https://doi.org/10.1175/MWR-D-17-0338.1.

Hong, S.Y., Noh, Y., Dudhia, J., 2006. A new vertical diffusion package with an explicit treatment of entrainment processes. Mon. Weather Rev. 134, 2318–2341. https://doi.org/10.1175/MWR3199.1.

Iacono, M.J., Delamere, J.S., Mlawer, E.J., Shephard, M.W., Clough, S.A., Collins, W.D., 2008. Radiative forcing by long lived greenhouse gases: calculations with the AER radiative transfer models. J. Geophys. Res.-Atmos. 113, D13103. https://doi.org/10.1029/2008JD009944.

Jaramillo, O.A., Borja, M.A., 2004. Wind speed analysis in La Ventosa, Mexico: a bimodal probability distribution case. Renew. Energy 29, 1613–1630. https://doi.org/10.1016/j.renene.2004.02.001.

Kain, J.S., 2004. The Kain-Fritsch convective parameterization: an update. J. Appl. Meteorol. Climatol. 43, 170–181. https://doi.org/10.1175/1520-0450(2004)043<0170:TKCPAU>2.0.CO;2.

Korobov, N.M., 1959a. Computation of multiple integrals by the method of optimal coefficients. Vestnik Moskow Univ. Sec. Math. Astr. Fiz. Him. 4, 19–25.

Korobov, N.M., 1959b. The approximate computation of multiple integrals. Dokl. Akad. Nauk SSSR 124, 1207–1210.

Lazić, L., Pejanović, G., Živković, M., 2010. Wind forecasts for wind power generation using the Eta model. Renew. Energy 35, 1236–1243. https://doi.org/10.1016/j.renene.2009.10.028.

Lu, X., McElroy, M.B., Kiviluoma, J., 2009. Global potential for wind-generated electricity. P. Natl. Acad. Sci. USA 106, 10933–10938. https://doi.org/10.1073/pnas.0904101106.

Mass, C., Ovens, D., 2010. WRF model physics: progress, problems, and perhaps some solutions. In: The 11th WRF users' Workshop, (Boulder, CO, 21–25 June, 2010).

Mathew, S., 2006. Wind Energy: Fundamentals, Resource Analysis and Economics. Springer, Berlin.

Moemken, J., Reyers, M., Feldmann, H., Pinto, J.G., 2018. Future changes of wind speed and wind energy potentials in EURO-CORDEX ensemble simulations. J. Geophys. Res.-Atmos. 123, 6373–6389. https://doi.org/10.1029/2018JD028473.

Mohandes, M.A., Rehman, S., Halawani, T.O., 1998. A neural networks approach for wind speed prediction. Renew. Energy 13, 345–354. https://doi.org/10.1016/S0960-1481(98)00001-9.

National Renewable Energy Laboratory, 2008. 20% Wind Energy by 2030: Increasing Wind energy's Contribution to U.S. Electricity Supply. U.S. Department of Energy, Washington, pp. 228.

Pan, L., Liu, Y., Knievel, J., Monache, L., Roux, G., 2018. Evaluations of WRF sensitivities in surface simulations with an ensemble prediction system. Atmosphere 9, 106. https://doi.org/10.3390/atmos9030106.

Pinson, P., Siebert, N., Kariniotakis, G., 2003. Forecasting of Regional wind Generation by a Dynamic Fuzzy-Neural Networks Based Upscaling Approach. European wind Energy Conference (EWEC). (Madrid, Spain, June).

Qian, Y., Yan, H., Hou, Z., Johannesson, G., Klein, S., Lucas, D., Neale, R., Rasch, P., Swiler, L., Tannahill, J., Wang, H., Wang, M., Zhao, C., 2015. Parametric sensitivity analysis of precipitation at global and local scales in the Community Atmosphere Model CAM5. J. Adv. Model. Earth Sy. 7, 382–411. https://doi.org/10.1002/2014MS000354.

Sfetsos, A., 2002. A novel approach for the forecasting of mean hourly wind speed time series. Renew. Energy 27, 163–174. https://doi.org/10.1016/S0960-1481(01)00193-8.

Skamarock, W., Klemp, J., Dudhia, J., Gill, D., Barker, D., Duda, M., Huang, X., Wang, W., Powers, J., 2008. A Description of the Advanced Research WRF Version 3, NCAR Technical Note. Mesoscale and Microscale Meteorology Division. National Center for Atmospheric Research, Boulder.

Stull, R., 1988. An Introduction to Boundary Layer Meteorology. Kluwer Academic Publishers, Dordrecht.

Tao, W., Simpson, J., 1993. Goddard cumulus ensemble model. Part I: model description. Terr. Atmos. Ocean. Sci. 4, 35–72.

Traiteur, J., Callicutt, D., Smith, M., Roy, S., 2012. A short-term ensemble wind speed forecasting system for wind power applications. J. Appl. Meteorol. Climatol. 51, 1763–1774. https://doi.org/10.1175/JAMC-D-11-0122.1.

Tymvios, F., Charalambous, D., Michaelides, S., Lelieveld, J., 2018. Intercomparison of boundary layer parameterizations for summer conditions in the eastern Mediterranean island of Cyprus using the WRF-ARW model. Atmos. Res. 208, 45–59. https://doi.org/10.1016/j.atmosres.2017.09.011.

Wang, Y., Yang, Y., Zhang, F., Yang, L., 2013. Improve the forecast of surface-layer wind in wind power farm with WRF-3DVAR. Adv. Mater. Res. 724, 480–484. https://doi.org/10.4028/www.scientific.net/AMR.724-725.480.

Wang, C., Duan, Q., Gong, W., Ye, A., Di, Z., Miao, C., 2014. An evaluation of adaptive surrogate modeling based optimization with two benchmark problems. Environ. Model. Softw. 60, 167–179. https://doi.org/10.1016/j.envsoft.2014.05.026.

Xiang, Y., Zhang, T., Liu, J., Lv, L., Dong, Y., Chen, Z., 2019. Atmosphere boundary layer height and its effect on air pollutants in Beijing during winter heavy pollution. Atmos. Res. 215, 305–316. https://doi.org/10.1016/j.atmosres.2018.09.014.

Yang, B., Qian, Y., Lin, G., Leung, L.R., Zhang, Y., 2012. Some issues in uncertainty quantification and parameter tuning: a case study of convective parameterization scheme in the WRF regional climate model. Atmos. Chem. Phys. 12, 2409–2427. https://doi.org/10.5194/acp-12-2409-2012.

Yang, B., Qian, Y., Berg, L., Ma, P., Wharton, S., Bulaevskaya, V., Yan, H., Hou, Z., Shaw, W., 2017. Sensitivity of turbine-height wind speeds to parameters in planetary boundary-layer and surface-layer schemes in the Weather Research and forecasting model. Bound.-Layer Meteorol. 162, 117–142. https://doi.org/10.1007/s10546-016-0185-2.

Zhang, D., Anthes, R.A., 1982. A high-resolution model of the planetary boundary layer–sensitivity tests and comparisons with SESAME-79 data. J. Appl. Meteorol. 21, 1594–1609. https://doi.org/10.1175/1520-0450(1982)021<1594:AHRMOT>2.0.CO;2.